High-resolution detection of underwater buried objects by acoustic vortex beams

Liwei Chen
School of Ocean and Civil Engineering
Shanghai Jiao Tong University
Shanghai, China
kraken1895@sjtu.edu.cn

Jun Fan
School of Ocean and Civil Engineering
Shanghai Jiao Tong University
Shanghai, China
fanjun@sjtu.edu.cn

Zhixiong Gong
School of Ocean and Civil Engineering
Shanghai Jiao Tong University
Shanghai, China
zhixiong.gong@sjtu.edu.cn

***Abstract*—Driven by applications such as seabed resource exploitation, submarine infrastructure maintenance, and maritime security, the detection of buried objects has become increasingly important. Acoustics remains the most effective underwater detection method; however, it still faces challenges for detecting buried targets due to the rapid attenuation of high-frequency waves in sediments and the limited resolution of low-frequency waves. Existing systems, such as synthetic aperture sonar and side-scan sonar, rely on echo amplitude and are often complex, expensive, and time-consuming. To balance penetration depth and resolution, we propose a buried object detection method based on the spatial phase information of acoustic vortex beams.**

Although acoustic vortex beams have been used in various applications, their spatial phase remains underexplored. The phase singularity, associated with superoscillations, offers high-resolution capability and has shown promise for underwater tasks. In this work, we present a numerical study of vortex-beam scattering of buried objects. Using the angular spectrum method (ASM), we establish a model that accounts for longitudinal waves in sand sediments with depth-dependent attenuation. The propagation of an arbitrary beam and the scattering problem from buried objects are numerically evaluated. A monostatic detection scenario is simulated, and the results obtained with a conventional in-phase array and the proposed vortex-phase array are compared. Results show that the spatial phase information of the scattering fields under acoustic vortex incidence holds potential for high-resolution buried target detection. This study demonstrates the feasibility of utilizing phase information for buried object detection and may pave the way for a new detection technique.

***Index Terms*—Vortex beam, Spatial phase, Buried target, Underwater detection.**

I. Introduction

With the increasing exploration and utilization of the ocean resources, the demand for detecting buried objects, such as cables and oil pipelines, has grown significantly [1] [2]. However, underwater detection of buried objects remains a persistent challenge, primarily due to the numerous interfering factors and low signal-to-noise ratio (SNR) of the backward scattering echoes. On one hand, the acoustic attenuation properties of the sediment layer prevent high-frequency acoustic fields from achieving sufficient penetration depth. On the other hand, lowering the frequency reduces the echo intensity, which in turn degrades detection resolution. To address this, a variety of detection methods have been developed for underwater buried target detection, including synthetic aperture sonar (SAS) [3] [4], which synthesizes a large virtual aperture through platform motion to achieve high resolution; parametric array sonar [5], which exploits the nonlinear self-demodulation effect to generate a highly directional, low-frequency beam from a small transducer aperture, offering both good penetration and high resolution; sub-bottom profilers [6], which employ low-frequency chirp signals to penetrate sediment layers and reveal subsurface stratification; and multibeam echo sounders [7], which map the seabed topography with high spatial resolution across a wide swath.

Collectively, these techniques primarily rely on the amplitude information and achieve enhanced resolution through complex hardware, sophisticated signal processing, and considerable time costs. In contrast, acoustic vortex beams have been demonstrated to possess spatial phase information with the potential for sub-diffraction imaging [8]. Characterized by a topological charge (or order) M, the phase varies azimuthally as $e^{iM\varphi}$ with φ the cylindrical azimuthal angle, which gives rise to a central phase singularity and a donut-shaped amplitude distribution (for helical cases where $M \neq 0$) on their propagation cross-section [9]. These unique spatial structures endow vortex beams with notable advantages for detection: (i) the spatial phase singularity enables high-resolution localization beyond the conventional diffraction limit [8] [10]; (ii) the phase structure is highly sensitive to perturbations caused by embedded objects, offering a distinct signature for detection [11]; and (iii) the beams can be synthesized at low frequencies using phased arrays, thus maintaining penetration depth while retaining high resolution based on spatial phase information. Consequently, acoustic vortex beams offer a new pathway for buried target detection by shifting the focus from amplitude-based to phase-based sensing [12] [13].

Motivated by these considerations, we conduct a numerical study on buried object detection using acoustic vortex beams. In Sec. II, a theoretical model is established for arbitrary acoustic propagation in a two-layer medium and the scattering from a rigid sphere at an arbitrary position. The scenarios of the in-phase transducer (conventional mode) and the vortex transducer (the proposed mode in this work) are calculated and compared, with the results presented in Sec. III. This work demonstrates that acoustic vortex beams have the potential for high-resolution detection of buried underwater targets.

Ongoing work is focused on further experimental validation and exploration of practical implementation.

II. Methods

In this section, we describe the method for modeling wave propagation in a two-layer medium and the associated scattering calculation for buried objects. The schematic is shown in Fig. 1(a), where a transducer immersed in water transmits acoustic beams toward the interface. The acoustic impedance contrast at the interface gives rise to both reflection and transmission (or refraction). Illuminated by the transmitted wave, a rigid sphere buried in the sediment (e.g., fine sand) generates scattered echoes. Here, we assume that both medium domains are infinite in extent. Even so, theoretically simulating and predicting the scattering problem remains challenging, even for plane wave incidence [14]. Therefore, we employ the ASM for the scattering calculation of arbitrary acoustic beams [15]. The ASM offers significant advantages in multi-layer medium problems, as it decomposes the acoustic field into angle-dependent plane waves, allowing the effects of reflection and refraction to be naturally integrated into the calculation. A brief description of the method is provided in the following subsections.

A. Wave propagation in two-layer medium based on ASM

It is assumed that both media are homogeneous and only longitudinal waves exist, with the water layer characterized by density ρ_1 and sound speed c_1, and the sediment layer by density ρ_2 and sound speed c_2. The refractive index is $n = c_1/c_2$. Based on ASM, in the water layer ($z \leq 0$), an arbitrary incident beam $p_i(x, y, z \leq 0)$ with frequency f, wavelength λ_1, wavenumber $k_1 = 2\pi/\lambda_1$ and the angular frequency $\omega = 2\pi f$ (omitting the time-dependence factor $e^{-i\omega t}$) is expressed as [15]:

$$p_i(x,y,z\leq 0) = \frac{1}{4\pi^2}\iint_{k_x^2+k_y^2\leq k_1^2} S_i\left(k_x,k_y\right)|_{z=-h} \times e^{ik_x x+ik_y y+ik_z(z+h)}dk_x dk_y, \tag{1}$$

where $k_z = \sqrt{(k_1^2 - k_x^2 - k_y^2)}$ and $S_i(k_x, k_y)|_{z=-h}$ is the angular spectrum derived from the source distribution at $z = -h$:

$$S_i\left(k_x,k_y\right)|_{z=-h} = \int_{-\infty}^{+\infty}\int_{-\infty}^{+\infty} p_i(x,y,z=-h) \times e^{-ik_x x-ik_y y}dxdy. \tag{2}$$

In Eq. (1), the integration region is set as $k_x^2 + k_y^2 \leq k_1^2$ to eliminate evanescent waves. One way of calculating the reflection and transmission is to use the obtained pressure field on the interface to propagate upwards and downwards, respectively. For convenience, we denote the beam vector $\mathbf{k^{(i)}}$ = (k_x,k_y,k_z) of an elementary plane wave in Eq.(1) as the angular-dependent form as $\mathbf{k^{(i)}} = k_1\ \mathbf{n^{(i)}}$ and the observation point $\mathbf{r} = (x, y, z)$. According to Snell's law and the continuity condition of the wavenumber at the interface, the unit direction vectors for incidence, reflection, and transmission are respectively [16]:

$$\begin{aligned}\mathbf{n^{(i)}} &= (\cos\alpha, \cos\beta, \cos\gamma),\\ \mathbf{n^{(r)}} &= (\cos\alpha, \cos\beta, -\cos\gamma),\\ \mathbf{n^{(t)}} &= \left(\frac{\cos\alpha}{n}, \frac{\cos\beta}{n}, \sqrt{1-\frac{1-\cos\gamma^2}{n^2}}\right).\end{aligned} \tag{3}$$

Therefore, beam vectors of reflection and transmission are derived and expressed as $\mathbf{k^{(r)}} = k_1\ \mathbf{n^{(r)}}$ = (k_x,k_y,-k_z) and $\mathbf{k^{(t)}} = k_2\ \mathbf{n^{(t)}}$ = ($k_x^{(t)}$,$k_y^{(t)}$,$k_z^{(t)}$), respectively. The corresponding pressure reflection and transmission coefficients for the elementary plane wave are given by [16]:

$$\begin{aligned}R\left(k_x,k_y\right) &= \frac{\rho_2 c_2\cos\theta_i - \rho_1 c_1\cos\theta_t}{\rho_2 c_2\cos\theta_i + \rho_1 c_1\cos\theta_t},\\ T\left(k_x,k_y\right) &= \frac{2\rho_2 c_2\cos\theta_i}{\rho_2 c_2\cos\theta_i + \rho_1 c_1\cos\theta_t},\end{aligned} \tag{4}$$

where the incidence angle and refraction angle are given respectively according to Eq. (3) as:

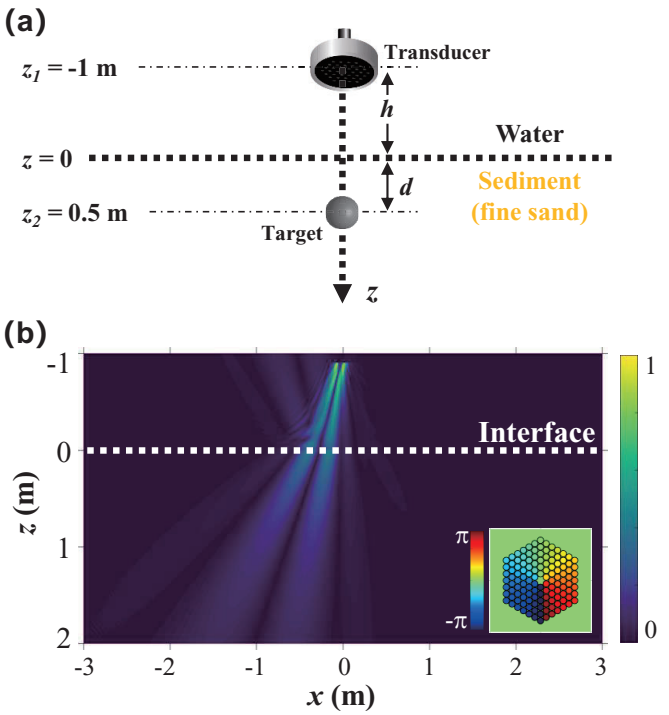

Fig. 1. (a) Schematic of the detection of underwater buried targets. The two media are separated at z = 0, with the transducer located h = 1 m above the interface and the target positioned d = 0.5 m below it. (b) The simulated propagation of a vortex beam through two media. The inset displays the initial phase distribution of the transducer, which emits at a tilt angle of 15° from the z axis.

$$\cos\theta_i = \cos\gamma,$$
$$\cos\theta_t = \sqrt{1 - \frac{1-\cos\gamma^2}{n^2}}. \tag{5}$$

When the incidence angle exceeds the critical angle $\theta_{ic} = \sin^{-1}(c_1/c_2)$, the reflection coefficient is set to 1 and the transmission coefficient to 0, denoted as $\hat{R}$ and $\hat{T}$, respectively. Then the reflection and transmission fields are expressed as follows:

$$p_r(x,y,z<0) = \frac{1}{4\pi^2} \iint\limits_{k_x^2+k_y^2\le k_1^2} \hat{R}\left(k_x,k_y\right) S_i\left(k_x,k_y\right)|_{z=0} \times e^{ik_1\mathbf{n^{(r)}}\cdot\mathbf{r}} dk_x dk_y, \tag{6}$$

$$p_t(x,y,z>0) = \frac{1}{4\pi^2} \iint\limits_{\substack{k_x^2+k_y^2\le k_1^2 \\ k_x^{(t)2}+k_y^{(t)2}\le k_2^2}} \hat{T}\left(k_x,k_y\right) S_i\left(k_x,k_y\right)|_{z=0} \times e^{ik_2\mathbf{n^{(t)}}\cdot\mathbf{r}} dk_x dk_y. \tag{7}$$

Now consider a transducer consisting of 127 cells arranged in a hexagonal pattern and a diameter D = 20 cm [12], a vortex beam with topological charge 1 is transmitted at a tilt angle of 15° from the z axis. The frequency is 70kHz and material parameters are provided in Table. I. Due to medium attenuation, the wavenumber in the transfer function in Eq. 7 is replaced by a complex wavenumber, with its real part equal to k_2 and its imaginary part representing the attenuation coefficient. Fig. 1(b) displays the results, and the inset shows the initial phase distribution of the transducer, where incident and reflection waves exist in the water domain ($z < 0$), and the transmission wave penetrates below the interface. This vortex beam M = 1 is reflected and refracted due to the interface. It is clearly shown that the beam axis with zero amplitude is deflected in the opposite direction, which is consistent with Snell's law. Since the acoustic impedances of the two media are close, most of the acoustic energy penetrates into the sediment; therefore, the transmitted intensity is larger than the reflected counterpart.

The standard ASM employs the fast Fourier transform (FFT), which achieves a short computation time while consuming significant computational resources. In this work, the Band-Extended ASM [17] is adopted, which extends the effective frequency band by resampling the angular spectrum and utilizes the non-uniform fast Fourier transform (NUFFT) to effectively reduce computational resource consumption and enable long-range acoustic propagation calculations. The implementation details can be found in [17].

B. Scattering calculation of a buried target

Similar to the propagation treatment in the previous subsection, the ASM-based scattering simulation also reduces the incident field to the sum of scattering from individual plane waves. For each plane wave, the partial wave method (PWM) can be used to solve for the scattering field from a buried rigid sphere of radius a. To facilitate the application of the PWM, we first establish a new coordinate system centered on the target, denoted as $\mathbf{r}' = (x', y', z') = (r', \theta', \phi')$ with $x' = x$, $y' = y$ and $z' = z - d$ for the case in Fig. 1(a). The propagation direction of each plane wave is known, that is represented as $\mathbf{k^{(t)}} = k_2\ \mathbf{n^{(t)}}$, while its amplitude is characterized by the angular spectrum. Therefore, the first step in solving the scattering problem is to obtain the acoustic field distribution in the new coordinate system, which has already been accomplished in Section.II-A. For the target at an arbitrary position, a general coordinate transformation of the angular spectrum is given in [15]. Accordingly, we obtain the transmission field distribution $p_t(x', y', z' = 0)$ and its angular spectrum:

$$S_t\left(k_x^{(t)}, k_y^{(t)}\right)|_{z'=0} = \int_{-\infty}^{+\infty}\int_{-\infty}^{+\infty} p_t(x', y', z'=0) \times e^{-ik_x^{(t)}x' - ik_y^{(t)}y'} dx' dy'. \tag{8}$$

Expanding the beam vector in spherical coordinates as $\mathbf{k^{(t)}} = (k_2, \theta_k, \phi_k)$, where $\cos\theta_k = k_z^{(t)}/k_2$ and $\phi_k = \arctan(k_y^{(t)}/k_x^{(t)})$. Eventually, the scattering field of the buried target in the sediment domain is expressed as [15]:

$$p_s(x,y,z\ge 0) = p_s(x',y',z'\ge -d) = \frac{1}{\pi}\sum_{n=0}^{\infty} i^n c_n h_n^{(1)}(k_2 r') \sum_{m=-n}^{n} Y_{nm}(\theta',\varphi') H_{nm}, \tag{9}$$

where c_n is the scattering coefficient of a rigid sphere given by $c_n = j_n'(k_2 a)/h_n^{(1)\prime}(k_2 a)$, $h_n^{(1)}$ is the spherical Hankel function of the first kind, and Y_{nm} are the normalized spherical harmonics [18]:

$$Y_{nm}(\theta',\varphi') = \sqrt{\frac{(2n+1)(n-m)!}{4\pi(n+m)!}} P_n^m(\cos\theta') e^{im\phi'}, \tag{10}$$

where P_n^m being the associated Legendre polynomials. All information about the transmitted field is encapsulated in the coefficients [15]:

$$H_{nm} = \iint\limits_{k_x^{(t)2}+k_y^{(t)2}\le k_2^2} S_t\left(k_x^{(t)}, k_y^{(t)}\right)|_{z'=0} Y_{nm}^*(\theta_k,\varphi_k) dk_x^{(t)} dk_y^{(t)}, \tag{11}$$

where the asterisk denotes the complex conjugate.

To obtain the scattering field in the upper medium, one can first compute the scattering field at the interface and then propagate it upward using the theory presented in Sec. II-A, which is essentially the inverse problem of the downward propagation of the incident field from the transducer. It should be noted that the method described in this section does not

TABLE I
MATERIAL PARAMETERS FOR WATER AND SEDIMENT

	Density (kg/m^3)	**Longitudinal speed** (m/s)	**Transverse speed** (m/s)	**Attenuation coefficient of longitudinal wave** (dB/λ)	**Attenuation coefficient of transverse wave** (dB/λ)
Water	1000	1500	-	0	-
Sediment (fine sand)	2053	1750	-	0.05	-

account for multiple scattering between the target and the interface.

III. Simulation Results

This section presents a numerical simulation of a realistic detection scenario using a monostatic configuration, where the beam is emitted and received at z_1 = -1m. The target is a rigid sphere of 4 cm diameter, and the remaining parameters are as given in the previous section and Table. I. The transducer is employed to generate a conventional Gaussian beam and an acoustic vortex beam by applying in-phase and first-order vortex phase modulation, respectively. The acoustic propagation for both operating modes, as well as the distribution of the transmitted field at the target plane and the received scattering field, are calculated and displayed in Figs. 2 and 3. For clarity, the amplitude is scaled in dB; for instance, $20\log_{10} p_s$ is shown for the scattered beam.

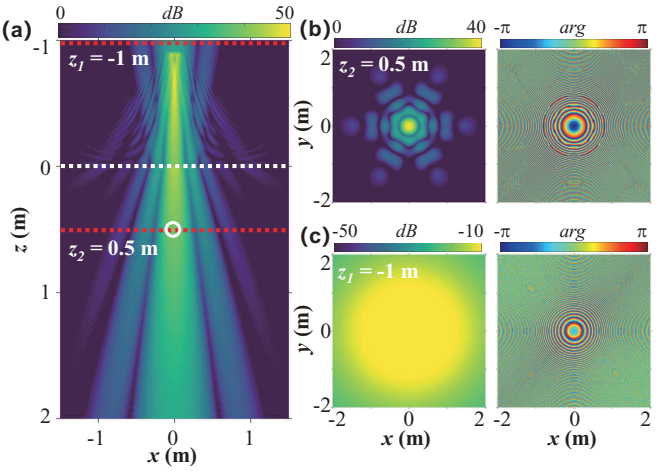

Fig. 2. Simulation results for the transducer operated under in-phase emission. (a) The beam propagation in the xz plane. (b) Amplitude and phase distributions of the transmitted field at the target plane (z_2 = 0.5m). (c) Amplitude and phase distributions of the scattering field at the receiver plane (z_1 = -1m).

For the Gaussian beam incidence, the main lobe and the side lobes in the hexagonal region can be clearly observed. Owing to the relatively small acoustic impedance contrast between the two media, a considerable portion of the acoustic energy penetrates into the sediment layer, achieving good penetration in the noise-free simulation. Nevertheless, the amplitude of the backward scattering field is weak. On one hand, the small size of the target (the dimensionless frequency $k_2 a = 5$) results in a weak scattering cross-section; on the other hand, acoustic attenuation in the medium and reflection at the interface further reduce the scattered amplitude. Similar behavior is observed under vortex beam illumination. Since part of the transducer energy is canceled by interference on the acoustic axis, the resulting echo amplitude is even weaker than that under plane-wave incidence. However, the scattering phase maps exhibit a distinct feature: a phase singularity appears at the center. This singularity arises from the rotational symmetry between the target and the acoustic field [19], which results from the interference of the scattered echo on the acoustic axis. Such spatial phase information in the scattering map can serve as an indicator of the presence of a target in the sediment layer, demonstrating that acoustic vortices possess the potential for high-resolution buried objects detection.

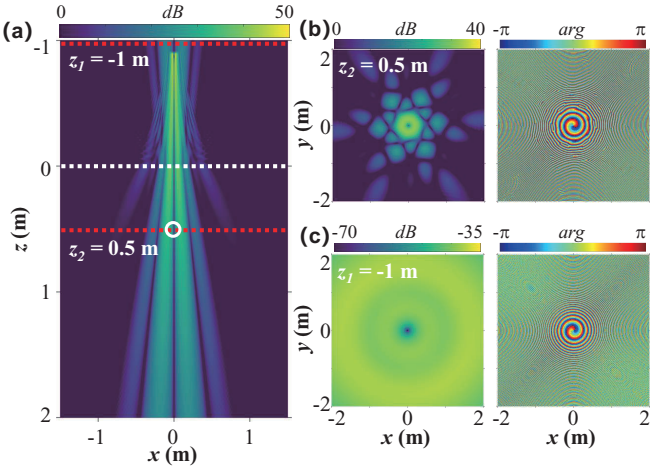

Fig. 3. Simulation results for the transducer operated under vortex-phase emission. (a) The beam propagation in the xz plane. (b) Amplitude and phase distributions of the transmitted field at the target plane (z_2 = 0.5m). (c) Amplitude and phase distributions of the scattering field at the receiver plane (z_1 = -1m).

IV. Conclusion

This work reports a detection method for underwater buried objects using the spatial phase information of a vortex beam. Based on ASM, the beam propagation and scattering calculation for an arbitrarily placed rigid sphere illuminated by an arbitrary beam in a two-layer medium are introduced. By comparing the scattering results obtained with the in-phase and vortex-phase transducers, we find that the spatial phase information of the scattering fields under acoustic vortex incidence holds potential for high-resolution buried target detection. It should also be noted that the SNR of vortex beams is weaker than that of conventional modes, which constitutes a limitation of this detection approach. Overall, this study presents a

method that utilizes vortex beams for underwater detection, demonstrates its potential for high-resolution buried target detection, and provides a new pathway for the application of spatial phase information in the field of detection.

ACKNOWLEDGMENT

Z. Gong thanks for the support from the National Natural Science Foundation of China (24Z990200542 and No. 12504522), the Joint Training Fund Project of Hanjiang National Laboratory (No. LP2024004), the XIAOMI Foundation, and the Shanghai Jiao Tong University [2030 Initiative, AI for Engineering Initiative, and the startup funding (WH220401017, WH22040121)].

REFERENCES

[1] S. Datta and S. Sarkar, "A review on different pipeline fault detection methods," Journal of Loss Prevention in the Process Industries, vol. 41, pp. 97–106, May 2016.

[2] S. K. Sinha and P. W. Fieguth, "Automated detection of cracks in buried concrete pipe images," Automation in Construction, vol. 15, no. 1, pp. 58–72, Jan. 2006.

[3] S. G. Kargl, K. L. Williams, T. M. Marston, J. L. Kennedy, and J. L. Lopes, "Acoustic response of unexploded ordnance (UXO) and cylindrical targets," in OCEANS 2010 MTS/IEEE SEATTLE, Seattle, WA: IEEE, Sep. 2010, pp. 1–5.

[4] S. G. Kargl, A. L. Espana, K. L. Williams, J. L. Kennedy, and J. L. Lopes, "Scattering from objects at a water–sediment interface: Experiment, high-speed and high-fidelity models, and physical insight," IEEE J. Oceanic Eng., vol. 40, no. 3, pp. 632–642, Jul. 2015.

[5] H. Zhou, S. H. Huang, and W. Li, "Parametric Acoustic Array and Its Application in Underwater Acoustic Engineering," Sensors, vol. 20, no. 7, p. 2148, Apr. 2020.

[6] M. Saleh and M. Rabah, "Seabed sub-bottom sediment classification using parametric sub-bottom profiler," NRIAG Journal of Astronomy and Geophysics, vol. 5, no. 1, pp. 87–95, Jun. 2016.

[7] K. Colbo, T. Ross, C. Brown, and T. Weber, "Colbo-2014-A review of oceanographic applications of water column data from multibeam echosounders," Estuarine, Coastal and Shelf Science, vol. 145, pp. 41–56, May 2014.

[8] T. Brunet, J.-L. Thomas, and R. Marchiano, "Transverse shift of helical beams and subdiffraction imaging," Phys. Rev. Lett., vol. 105, no. 3, p. 034301, Jul. 2010.

[9] M. V. Berry, "Dislocations in wave trains," Proc. R. Soc. Lond. A, vol. 336, no. 1605, pp. 165–190, Jan. 1974.

[10] X. Li, X. Jiang, and D. Ta, "Composite Orbital Angular Momentum for Super-resolution Ultrasound Imaging," Phys. Rev. Lett., vol. 136, no. 11, p. 114002, Mar. 2026.

[11] P. L. Marston, "Phase and amplitude evolution of backscattering by a sphere scanned through an acoustic vortex beam: Measured helicity projections," The Journal of the acoustical Society of America, vol. 148, no. 2, Art. no. 2, 2020.

[12] L. Chen, J. Fan, Z. Gong, "Extraction of the direct scattering of a sphere in a vortex beam: Theory and experiment,"JASA Express Lett, in press, https://doi.org/10.1121/10.0043233.

[13] Z. Gong, L. Chen, J. Fan, B. Wang, F. Zhou, K. Zhao, J. Li, "Method for target detection based on correlation analysis of spatial phase in an acoustic vortex," U.S. Patent 12,510,661 B2, Dec 30, 2025.

[14] G. C. Gaunaurd and H. Huang, "Acoustic scattering by a spherical body near a plane boundary," The Journal of the acoustical Society of America, vol. 96, no. 4, pp. 2526–2536, Oct. 1994.

[15] O. A. Sapozhnikov and M. R. Bailey, "Radiation force of an arbitrary acoustic beam on an elastic sphere in a fluid," The Journal of the acoustical Society of America, vol. 133, no. 2, pp. 661–676, Feb. 2013.

[16] G. V. Frisk, Ocean and Seabed Acoustics: A Theory of Wave Propagation. Englewood Cliffs, NJ: Prentice-Hall, 1994, p.34-41.

[17] W. Zhang, H. Zhang, and G. Jin, "Band-extended angular spectrum method for accurate diffraction calculation in a wide propagation range," Opt. Lett., vol. 45, no. 6, p. 1543, Mar. 2020.

[18] G. B. Arfken, H. J. Weber, and F. E. Harris, Mathematical Methods for Physicists, 7th ed. Amsterdam, The Netherlands: Elsevier/Academic Press, 2013, p.756-757.

[19] P. L. Marston, "Scattering of a bessel beam by a sphere: II. Helicoidal case and spherical shell example," The Journal of the acoustical Society of America, vol. 124, no. 5, pp. 2905–2910, Nov. 2008.